



Original Research Article

Species coexistence by front pinning

Paris Kyriazopoulos^{a,*}, Jonathan Nathan^b, Ehud Meron^{b,c}^a Laboratoire de Mathématiques, Université de Paris-Sud (Bât. 425), Orsay cedex 91405, France^b Department of Solar Energy and Environmental Physics, Blaustein Institutes for Desert Research, Ben-Gurion University, Sede Boqer Campus 84990, Israel^c Department of Physics, Ben-Gurion University, Beer Sheva 84105, Israel

ARTICLE INFO

Article history:

Received 29 November 2013

Received in revised form 28 March 2014

Accepted 2 May 2014

Available online 21 June 2014

Keywords:

Plant communities

Trait tradeoff

Species competition

Species coexistence

Vegetation pattern formation

Localized structures

Homoclinic snaking

ABSTRACT

The spatial competition between two plant species that make different compromises in capturing soil water and sunlight is studied using a mathematical model. A precipitation range along the rainfall gradient is identified where two alternative stable states coexist. The first state describes a uniform distribution of a plant species that specializes in capturing soil water, whereas the second state describes a periodic pattern of a species that specializes in capturing light. We show that this bistability range generally divides into three parts according to the dynamics of the front or ecotone that separates the two plant populations: a low precipitation range where the superior competitor for water displaces the superior competitor for light, a high precipitation range where the displacement is reversed, and an intermediate range where neither species displaces the other. While in the low and high precipitation ranges one species outcompetes the other, the intermediate range allows for species coexistence in the form of a multitude of stable localized solutions consisting of fixed domains of one species in areas otherwise occupied by the other species. These localized solutions can only be realized when one of the alternative stable states is spatially patterned. We further study two factors that affect the size of the species coexistence range: the strength of the competition for light and the form of the tradeoff between the competitive abilities to capture water and light.

© 2014 Elsevier B.V. All rights reserved.

1. Introduction

Water-limited vegetation is generally patchy. According to the traditional view, vegetation patchiness is a result of an underlying physical template, often formed by slow geologic and geomorphologic processes, that creates favorable vegetation-growth areas (Sheffer et al., 2013). A different view of vegetation patchiness has been motivated by recent field observations of banded vegetation and other forms of regular vegetation patterns in nearly homogeneous landscapes (Tongway et al., 2001; Deblauwe et al., 2008). According to this view vegetation patterns can result from small-scale biomass-water feedbacks that give rise to self-organization at large scales even in spatially uniform systems (Rietkerk and van de Koppel, 2008; Meron, 2012). Mathematical models that capture these feedbacks have been very instrumental in understanding the causes of self-organized vegetation patchiness and the specific forms it takes along the rainfall gradient (Borgogno et al., 2009). Studies of such models

have first identified five basic vegetation states along the rainfall gradient (von Hardenberg et al., 2001; Rietkerk et al., 2002): uniform vegetation, hexagonal gap patterns, stripes or labyrinthine patterns, hexagonal spot patterns, and bare soil, which are in good agreement with field observations. They further suggest richer forms of self-organized vegetation patchiness: disordered spatial mixtures of basic states in bistability ranges, and amorphous patches that span wide patch-size distributions under conditions of global competition (von Hardenberg et al., 2010; Meron, 2012).

Most model studies have considered a single plant species, overlooking the large plant communities that generally exist in water-limited landscapes (Shachak et al., 2005). The tendency of water-limited ecosystems to self-organize in patchy landscapes raises the question: what impact does vegetation pattern formation have on species coexistence and diversity? This is a significant question, particularly nowadays, when transitions between different vegetation states become more likely due to the ongoing global climate change and the environmental fluctuations associated with it (Field et al., 2013). Understanding the response of plant communities to such transitions is important for maintaining the diversity of water-limited ecosystems and securing their function and stability.

* Corresponding author at: Ath. Diakou 4 Agios Pavlos, Thessaloniki 55438, Greece. Tel.: +30 6932223755.

E-mail address: p.p.kyriazopoulos@gmail.com (P. Kyriazopoulos).

Very few model studies have addressed the interaction between different species in water-limited vegetation, taking into account mechanisms of vegetation pattern formation. All of them have considered a pattern-forming species that acts as an ecosystem engineer (Jones et al., 1994, 1997) by concentrating the water resource, thereby facilitating the growth of the other species understory (Pugnaire and Luque, 2001; Holzapfel et al., 2006; Maestre et al., 2005). One set of studies has focused on the interplay between biomass-water feedbacks that have opposite effects on the soil-water distribution, and the development ecosystem engineering under conditions of water stress (Gilad et al., 2007a,b; Meron, 2012). Two other studies focused on species coexistence where a pattern-forming ecosystem engineer is an inferior competitor that survives the competition with a superior competitor because of the highly dispersive character of the latter (Baudena and Rietkerk, 2013; Nathan et al., 2013).

In this paper we propose a new pattern-formation mechanism of species coexistence that is based on a generic mathematical property associated with bistability of a uniform state and a periodic-pattern state – the possible existence of a multitude of stable localized structures (or homoclinic orbits in an appropriately defined dynamical system) (Knobloch, 2008). These structures consist of confined domains of the patterned state in a background of the other, spatially uniform, alternative stable state, and vice versa. Their existence is related to the dynamics of the transition zones that separate the two alternative stable states, i.e. the fronts that are bi-asymptotic to the two states (Pomeau, 1986). When the two alternative stable states are spatially uniform the fronts propagate in one direction or another, except for a particular value of the control parameter (the Maxwell point) at which the fronts are stationary (Pismen, 2006). By contrast, when one of the alternative stable states is spatially patterned there might exist a finite range of the control parameter within which fronts are stationary or pinned. It is within this range that localized structures are found. The mathematical property described above is commonly referred to as “homoclinic snaking”, because of the snake-like forms of the solution branches that describe the localized structures in the corresponding bifurcation diagrams (Knobloch, 2008). Localized structures of this kind were found also in a vegetation model for a single plant species in a bistability range of periodic vegetation pattern and bare soil (Lejeune et al., 2002; Zelnik et al., 2013).

To study species coexistence associated with bistability of uniform and patterned states we consider two plant species in water limited ecosystems that are related to one another by a tradeoff between investment in growing taller shoots and investment in increasing root-to-shoot ratio. Taller plants have an advantage in capturing light whereas plants with higher root-to-shoot ratios have an advantage in capturing soil water. We study the interaction between these two species along a rainfall gradient using a modified version of the vegetation model introduced by Gilad et al. (2004) that includes inter-specific competition for light. Since the proposed coexistence mechanism is based on a generic mathematical property of bistable pattern-forming systems, the results presented here may be applicable to many other contexts of ecological communities.

2. Modeling community dynamics

The model we study is based on the multi-species vegetation model introduced by Gilad et al. (Gilad et al., 2007a; Meron, 2011). The Gilad et al. model describes the evolution of a plant community in a water limited system where species interact through competition for water. In its most general form the model consists of a system of integro-differential equations that models non-local water uptake by laterally extended root zones. Here we study a

modified version of this model that takes into account competition for light too, but simplifies it in other respects.

2.1. Model equations

The original model consists of equations for the above-ground biomass densities B_i of N interacting species ($i = 1, \dots, N$), the soil water content per unit ground area W and the height of a surface-water layer above ground level H . We simplify it first by assuming that the infiltration rate of surface water into the ground is approximately constant, independent of the plants' biomass. Quite often the infiltration rate in bare soil is lower than that in vegetated soil because it is covered by physical and biogenic crust that makes the infiltration slower (Eldridge and Zaady, 2012). This effect can be negligible in sandy soils which are often uncrusted. When the infiltration rate is constant the equation for H decouples from the equations for W and the B_i s and the variable H can be eliminated (Zelnik et al., 2013). The model equations in one dimension (1d) then read

$$\frac{\partial B_i}{\partial t} = \Lambda_i(B)G_{B_i}(B_i, W)(1 - B_i/K_i)B_i - M_i B_i + D_{B_i} \frac{\partial^2 B_i}{\partial x^2}, \quad (2.1a)$$

$$\frac{\partial W}{\partial t} = P - LW - G_W(B)W + D_W \frac{\partial^2 W}{\partial x^2}, \quad (2.1b)$$

where $B = (B_1, \dots, B_N)$ and x represents a 1d lateral direction. The nonlinear growth rate of the i th species includes a water dependent factor, $G_{B_i}(B_i, W)$, that represents water uptake by the plants' roots, and a biomass dependent factor, $\Lambda_i(B)$, that accounts for light attenuation by competing plant species. The growth rate of grown plants is also limited by genetic factors, such as stem strength, whose effects are lumped in the parameter K_i . In the case of annuals K_i can also represent the limited size a plant can develop in its life cycle. Biomass growth is also limited by mortality and grazing that are represented by the parameter M_i . Spatial biomass expansion is accounted for by a diffusion term that represents short-distance seed dispersal or clonal growth, where the “biomass diffusivity”, D_{B_i} , is assumed to be a constant parameter. In the soil water Eq. (2.1b), the parameter P represents the precipitation rate while L represents the evaporation rate, which in general may also depend on the above-ground biomass to account for reduced evaporation by shading. The factor $G_W(B)$ is the rate of water uptake by the plants' roots, and its biomass dependence reflects the increase in the root-zone size as the above-ground increases, i.e. the root-to-shoot ratio. Lastly, the term $D_W \partial^2 W / \partial x^2$ models water transport in a non-saturated soil with D_W being a diffusivity constant.

2.2. Competition for water

Plants compete for water through water uptake by their roots. For laterally extended root zones the uptake is nonlocal and is captured by the following form (Gilad et al., 2007b),

$$G_W(x, t) = \sum_{i=1}^N \Gamma_i \int g_i(x', x, t) B_i(x', t) dx',$$

where the kernel $g_i(x', x, t)$ represents the roots architecture, and the integration is over the root zone of plants located at x . We use the form

$$g_i(x, x', t) = \frac{1}{\sigma_i \sqrt{2\pi}} \exp\left(-\frac{|x - x'|^2}{2\sigma_i^2(1 + E_i B_i(x, t))^2}\right),$$

where E_i quantify the root augmentation per unit of above-ground biomass, which is a measure of the root-to-shoot ratio. Note that

$g_i(x, x', t) \neq g_i(x', x, t)$ because of the biomass dependence. The biomass growth rates have nonlocal forms too

$$G_{B_i}(x, t) = \int g_i(x, x', t)W(x', t)dx',$$

since they depend on water availability at all points where the plants' roots extend to.

Another simplification we make here is the assumption of laterally confined root zones. This assumption is consistent with the assumption of sandy soil (used to eliminate the surface water variable) because its high soil-water diffusivity combined with gravity gives an advantage to plants with roots extending vertically to deep soil layers. To implement this simplification we take the limits $\sigma_i \rightarrow 0$ (vanishingly small lateral root sizes of seedlings) in which the biomass growth rates and the water uptake rate become

$$G_{B_i}(B_i, W) = (1 + E_i B_i)W, \tag{2.2}$$

$$G_W(B) = \sum_{i=1}^N \Gamma_i B_i (1 + E_i B_i). \tag{2.3}$$

Competition for water can be inter-specific, occurring between individuals that belong to different plant species, or intra-specific, occurring between individuals that belong to the same plant species. Inter-specific competition is captured by the rate forms (2.2) and (2.3), which give advantage to species with higher E_i values, for they grow faster and leave less water for other species. Intra-specific competition is also captured but in a spatial context; the biomass density of a given species, B_i , does not resolve the different individuals that contribute to the biomass $B_i(x, t)dx$ within a small length element (area element in 2d) around the point x , but does distinguish between groups of individuals that occupy different length elements.

An important manifestation of intra-specific competition occurring between distinct spatial locations is spatial instabilities leading to vegetation patterns. Intra-specific competition leading to vegetation pattern formation is captured by the soil-water diffusion term and the water uptake term in (2.1b), which together with the water-dependent biomass growth rate form a positive feedback between local vegetation growth and water transport towards the growing vegetation. The water uptake by a patch of growing vegetation depletes the local soil water content and induces water diffusion from the patch surroundings. The supply of water by diffusion accelerates the vegetation growth in the patch, but also inhibits the growth in the patch surroundings, thereby favoring the growth of nonuniform perturbations and the formation of vegetation patterns.

2.3. Competition for light

When the productivity of a system is sufficiently high, taller plants reduce the availability of light to shorter plants by shading. The positive feedback between shoot growth and light availability results in an inter-specific competition for light that can lead to the dominance of the taller plant species (Tilman, 1982).¹ To capture competition for light we introduce the following form for the biomass growth rate of the i th plant species:

$$\Lambda_i(B) = \Omega_i \left(1 - \frac{\sum_{j \neq i} B_j}{\sum B_j + h} \right). \tag{2.4}$$

¹ Note that the biomass variable represents the overall biomass per unit area of the i th species, irrespective of the number of individuals contributing to it. Thus, the modeling approach used here does not resolve local intra-specific competition. However, it does take into account nonlocal intra-specific competition as explained in Section 2.2.

Here, Ω_i represents the growth rate of the i th species in the absence of competitors and h is a positive constant serving as a reference value for the total biomass beyond which light becomes a limiting resource for small plants.

2.4. Trait tradeoff

We consider species that make different tradeoffs between investment in shoot growth and investment in root growth. To define this tradeoff we quantify the investment in shoot growth by the parameter K and the investment in root growth by the parameter E , and describe them parametrically as

$$\begin{aligned} K &= K(\chi; \alpha) = K_{\min} + (K_{\max} - K_{\min})(1 - \chi)^\alpha, \\ E &= E(\chi; \alpha) = E_{\min} + (E_{\max} - E_{\min})\chi^\alpha, \end{aligned} \tag{2.5}$$

where $\chi \in [0, 1]$ is a dimensionless tradeoff parameter, which describes the community of interest. The i th species is defined by the pair (K_i, E_i) or, alternatively, by the point χ_i on the tradeoff axis.² The parameter $\alpha > 0$ delimits tradeoff curves in the rectangle $R = [E_{\min}, E_{\max}] \times [K_{\min}, K_{\max}]$ that describe different species pools as Fig. 1 illustrates.

2.5. Parameter values and units

The model equations are presented in dimensional form. The dimensions of the state variables, the independent space and time variables, and the model parameters are presented in Table 1. Table 1 also displays the numerical values used in this study for the various parameters. No attempt has been made to fit the parameter values to a specific ecosystem; the values used rather represent the correct orders of magnitude for herbaceous or small woody vegetation (e.g. shrubs) in general. For simplicity, in what follows we drop the units notation from numerical values of parameters and variables and refer the reader to Table 1 for that purpose.

3. Stationary solutions

We consider the system (2.1) for two interacting plant species, that is, the set of equations

$$\begin{aligned} \frac{\partial B_1}{\partial t} &= \Lambda_1(B)G_{B_1}(B_1, W)(1 - B_1/K_1)B_1 - M_1 B_1 + D_{B_1} \frac{\partial^2 B_1}{\partial x^2}, \\ \frac{\partial B_2}{\partial t} &= \Lambda_2(B)G_{B_2}(B_2, W)(1 - B_2/K_2)B_2 - M_2 B_2 + D_{B_2} \frac{\partial^2 B_2}{\partial x^2}, \\ \frac{\partial W}{\partial t} &= P - LW - G_W(B)W + D_W \frac{\partial^2 W}{\partial x^2}, \end{aligned} \tag{3.1}$$

where G_{B_i} , $G_W(B)$ and $\Lambda_i(B)$ are given, respectively, by (2.2), (2.3) and (2.4) for $i = 1, 2$ and $B = (B_1, B_2)$. We study this system on a finite spatial interval imposing periodic boundary conditions. Analogous results can be obtained for the homogeneous Neumann boundary conditions. Since we are primarily interested in species that make different compromises in their investments in above and below-ground biomass, we characterize them by χ values close to zero and close to unity. Specifically, we assign a value $\chi_1 \ll 1$ to the species with biomass B_1 , and a value $\chi_2 = 1$ to the species with biomass B_2 . The χ_1 species represents a superior competitor for light (high K and low E) while the χ_2 species represents a superior competitor for water (high E and low K). The two species are kept identical in regard to all other trait parameters.

² More precisely, the point χ_i , including a small length element $\Delta\chi$ around it, describes a functional group whose species share the same values, K_i and E_i , of the functional traits K and E .

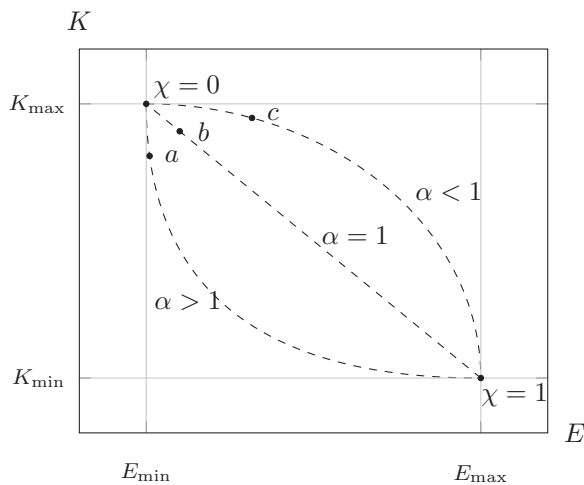


Fig. 1. The tradeoff between soil-water capture, as quantified by E , and sunlight capture, as quantified by K (see (2.5)). Shown are three typical tradeoff lines in the rectangle $[E_{\min}, E_{\max}] \times [K_{\min}, K_{\max}]$ that are parameterized by $\chi \in [0, 1]$ and represent different species pools: diagonal ($\alpha = 1$), subdiagonal ($\alpha > 1$) and supdiagonal ($\alpha < 1$). The solid circles represent the two species to be considered, $\chi = 0$ (biomass B_1) and $\chi = 1$ (biomass B_2) for most of the studies, and $\chi < 1$ (the circles a, b, c) and $\chi = 1$ for studying the effect of the species pools (or α) on species coexistence (Section 5.2).

3.1. Uniform states

The system (3.1) possesses three types of uniform equilibria $U = (B_1, B_2, W)$:

- The trivial bare soil state $U_0 = (0, 0, W_0)$
- Pure population states $U_1^* = (B_1^*, 0, W_1^*)$ and $U_2^* = (0, B_2^*, W_2^*)$,
- Coexistence states of the form $\bar{U} = (\bar{B}_1, \bar{B}_2, \bar{W})$.

A linear stability analysis of these solutions is described in Appendix A. The results are summarized in the bifurcation diagram in Fig. 2, which shows the existence and stability ranges of selected stationary uniform states (excluding, in particular, the coexistence states which are unstable in the parameter range considered here). At very low precipitation values P , the bare-soil state, U_0 , is the only stable state. At sufficiently high P values there is a bistability range of the two uniform pure-population states, U_1^* and U_2^* . The latter loses stability at $P = P_2^M$ to a mixed-population state, leaving the pure-population state

U_1^* of the superior light competitor, $\chi_1 \ll 1$, as the only stable state in the range $P > P_2^M$. The stability range of the uniform state U_1^* is bounded below by a nonuniform stationary instability at P_1^T (see Fig. 2) that leads to a stationary periodic pattern. The uniform state U_2^* can also go through such an instability but at lower precipitation values. These are Turing instabilities (Turing, 1952) that in the present context require strong water uptake and fast soil-water diffusion relative to the rate of seed dispersal or clonal growth.

3.2. Spatially periodic states

To study the solutions that appear below the Turing instability at P_1^T we resort to numerical continuation and stability methods. Applying the continuation package AUTO (Doedel et al., 2002) with P as a bifurcation parameter we find the spatially periodic solution $U_{1,p}^* = (B_1^*(x), 0, W_1^*(x))$ that emanates from the U_1^* uniform-solution branch at P_1^T , and additional periodic solutions, not shown in Fig. 2, that emanate from the U_2^* branch at $P < P_1^T$. All solution branches reconnect to the U_1^* branch at lower P values. Fig. 2 also shows typical spatial biomass and soil-water profiles associated with these periodic solutions. As Fig. 2 indicates there is a wide bistability range of the uniform U_2^* state and the periodic $U_{1,p}^*$ pattern.

3.3. Localized states

As discussed in the Introduction section, bistability ranges of uniform and periodic-pattern states often give rise to stable localized solutions involving confined domains of one state in a system otherwise occupied by the alternative state. In the bistability range of the uniform U_2^* state and the periodic $U_{1,p}^*$ pattern such solutions correspond to confined patterns of the species χ_1 that specializes in capturing light in an otherwise uniform distribution of the species χ_2 that specializes in capturing soil water. The bifurcation diagram in Fig. 3 shows the solution branches associated with several localized solutions of increasing size and their stability properties. The localized solution branches snake up towards the periodic-pattern solution, acquiring an additional hump in each turn as the panels (a–f) show. Unlike some other examples of homoclinic snaking (Knobloch, 2008; Beck et al., 2009; Dawes, 2008) there appears to be a single family of localized solutions containing both odd and even numbers of humps (Bortolozzo et al., 2008), rather than two distinct families of odd solutions and of even solutions.

Table 1
A list of dimensional quantities (state variables, space and time coordinates, parameters), their units, meanings and numerical values. The subscript i refers to traits of the i th species.

Quantity	Units	Description	Value
B_i	kg/m ²	Biomass density	–
W	kg/m ²	Soil water density	–
x	m	Space coordinate	[0,5]
t	yr	Time coordinate	–
K_{\min}	kg/m ²	Minimal standing biomass limit	0.5
K_{\max}	kg/m ²	Maximal standing biomass limit	3
E_{\min}	(kg/m ²) ⁻¹	Minimal root augmentation per unit biomass	0.5
E_{\max}	(kg/m ²) ⁻¹	Maximal root augmentation per unit biomass	3
χ_1	–	Tradeoff parameter for superior light competitor	$\chi_1 \ll 1$
χ_2	–	Tradeoff parameter for superior water competitor	1
L	yr ⁻¹	Soil water evaporation rate	6
P	kg/m ² yr ⁻¹	Precipitation rate	Variable
h	kg/m ²	Reference total-biomass value for light to become a limiting resource	Variable
D_W	m ² /yr	Soil water diffusivity	6.25×10^{-1}
$D_{B_1} = D_{B_2}$	m ² /yr	Seed dispersal coefficient	6.25×10^{-5}
$M_1 = M_2$	yr ⁻¹	Biomass decay rates	2
$\Omega_1 = \Omega_2$	(kg/m ²) ⁻¹ yr ⁻¹	Biomass growth rate per unit soil water	0.1
$\Gamma_1 = \Gamma_2$	(kg/m ²) ⁻¹ yr ⁻¹	Soil water uptake rate per unit biomass	2.2

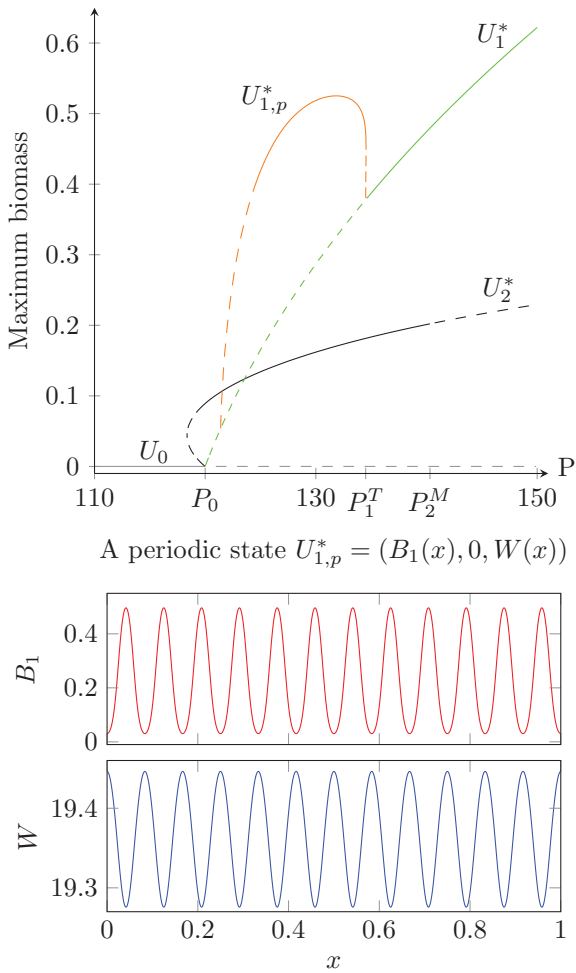


Fig. 2. Bifurcation diagram (top) showing biomass–precipitation solution branches for the bare-soil state, U_0 , the two pure-population uniform states, U_1^* and U_2^* , and for the pure-population periodic-pattern state, $U_{1,p}^*$, for which the maximum biomass is plotted. Solid (dashed) lines denote stable (unstable) states. The two uniform states bifurcate from the bare-soil state at $P = P_0$. The periodic-pattern state bifurcates from the corresponding uniform state at $P = P_1^T$ and reconnects to it at a lower precipitation value. The spatial dependence of the biomass $B_1(x)$ and soil-water $W(x)$ associated with the periodic-pattern state $U_{1,p}^* = (B_1(x), 0, W(x))$ are shown at the bottom part of the figure. Note the existence of a bistability precipitation range of the uniform U_2^* solution and of the periodic $U_{1,p}^*$ solution. Parameters are as in Table 1 with $\chi_1 = 0$. Note that the spatial domain is scaled down by a factor 5.

4. Species coexistence and spatial displacement

The multiplicity of stable localized solutions implies the possible coexistence of the two species in the same area and under the same environmental conditions. This is a new species coexistence mechanism in uniform environments associated with pattern formation (Nathan et al., 2013). The mechanism is related to the inability of either species to displace the other, or to the pinning of the front that is bi-asymptotic to U_2^* and $U_{1,p}^*$. The front pinning can be viewed as resulting from the interplay between competition for light and water; because of the different tradeoffs the two species make in capturing these resources, each species has an advantage and disadvantage in attempting to displace the other, which balance one another. The physical and ecological processes that maintain this balance over a precipitation range rather than at a single precipitation value (the Maxwell point) are not clear yet.

The localized structures occupy a limited subrange within the bistability precipitation range of the two pure-population states U_2^*

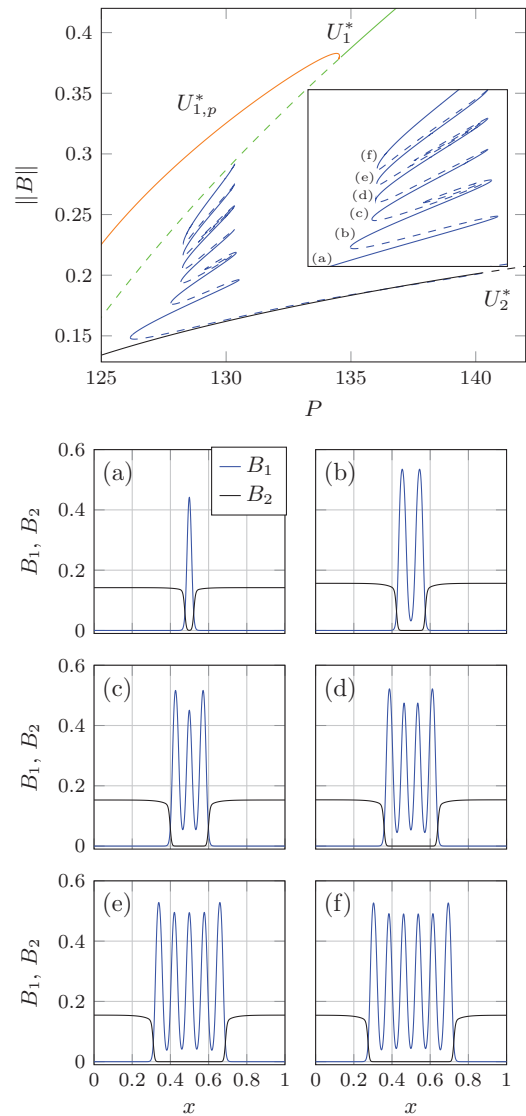


Fig. 3. A bifurcation diagram that includes localized solution branches (top). The vertical axis is chosen here to be the L_2 norm of the biomass variables defined as $\|B\| = (\int B_1^2 + B_2^2 dx)^{1/2}$. The inset shows a blow up of the localized solution branches labeled in ascending order of localized-solution sizes as the spatial solution forms in panels (a–f) show. The blue and black graphs denote B_1 and B_2 , respectively. Parameters are as in Table 1 except that the spatial domain is scaled down by a factor 5. (For interpretation of the references to color in this figure legend, the reader is referred to the web version of the article.)

and $U_{1,p}^*$. Outside this subrange, but still within the bistability range, one species displaces the other as Fig. 4a, d show. At relatively high precipitation water is no longer a strong limiting factor and competition for light becomes more important. As a result, the $U_{1,p}^*$ state, which represents a periodic pattern of the better competitor for light, invades into areas occupied by the U_2^* state (Fig. 4d). At relatively low precipitation the vegetation is less dense and light is no longer a strong limiting factor. As a result the competition for water becomes more important, and the U_2^* state, which represents the better competitor for water, invades into areas occupied by the $U_{1,p}^*$ state (Fig. 4a).

Within the range of localized structures there is a significant subrange in which the only stable localized structure is a single hump solution, and a smaller subrange where only single-hump and two-hump solutions are stable. In these subranges, large initial domains of the patterned state $U_{1,p}^*$ first contract but do not disappear; they rather converge to a single-hump or two-hump

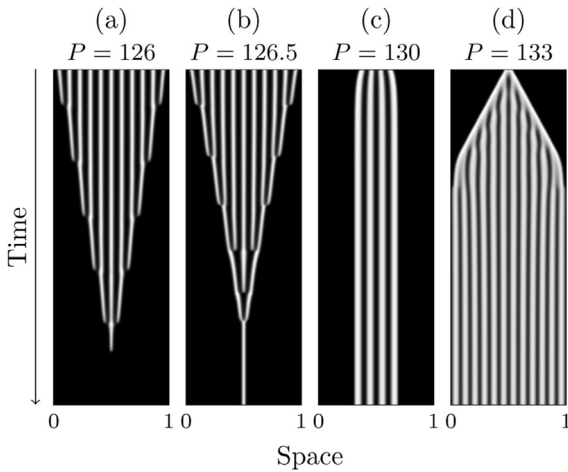


Fig. 4. Space-time plots showing different dynamical behaviors within the bistability range of the U_2 state (uniform distribution of the χ_2 species) and the $U_{1,p}$ state (periodic pattern of the χ_1 species). At low precipitation outside the range of stable localized solutions the U_2 state invades into the $U_{1,p}$ state, leading asymptotically to a U_2 state occupying the whole domain (a). At higher precipitation the U_2 state still invades into large domains of the $U_{1,p}$ state, but the invasion process culminates in a stable single-hump localized solution (b). At yet higher precipitation a multitude of stable localized solutions exists and any localized initial condition converges to a nearby localized solution (c). Finally, at sufficiently high precipitation the $U_{1,p}$ state invades into the U_2 state, leading asymptotically to a $U_{1,p}$ state occupying the whole domain (d). Parameters are as in Table 1 with P as specified in the figure.

solutions, as Fig. 4b demonstrates. Most of the remaining subrange of stable localized solutions contains a high multiplicity of localized structures of increasing sizes. Within this subrange most initial conditions have “nearly” stable localized solutions to which they converge on a relative short time scale without noticeable contraction or expansion, as Fig. 4c demonstrates.

5. Factors controlling species coexistence

The precipitation range of stable localized structures defines the species coexistence range; domains of periodic distributions of the χ_1 species embedded in an otherwise uniform distribution of the χ_2 species or vice versa. The size of this range naturally depends on model parameters that affect the competition for light and water. Two parameters of this kind are investigated below, the reference biomass value h , which controls the intensity of the competition for light, and the species pool parameter α .

5.1. Competition for light

The strength of the competition for light can be controlled using the parameter h that appears in Eq. (2.4) for the biomass growth rate $\Lambda_i(B)$. Smaller values of h imply lower biomass growth rate for the shaded species and thus a stronger competition effect. Conversely, as h is increased the competition for light becomes weaker and completely disappears when $h \rightarrow \infty$ as Λ_i approaches a constant value independent of B . Fig. 5 shows the effect of increasing h on the species-coexistence range as measured by the existence range of the one-hump solution. Apart from a small range of low h values, the species-coexistence range is found to decrease as h is increased. The reduction in the coexistence range occurs mostly through a shift of its low precipitation edge to higher precipitation values. As the competition for light decreases the advantage of χ_1 over χ_2 weakens and χ_2 is able to displace χ_1 . The balance between the two competitive abilities (capturing light vs. capturing water) that leads to front pinning, is then regained only at higher precipitation values.

5.2. Species pool

We recall that E and K are the biotic parameters that control the competitive abilities to capture water and light, respectively. The actual values that these parameters can take in the rectangle $R = [E_{\min}, E_{\max}] \times [K_{\min}, K_{\max}]$ are determined by the tradeoff curves obtained for different α values, as Fig. 1 illustrates. Each curve is parameterized by $\chi \in [0, 1]$ and represents a different species pool.

In order to study how does the species pool affect coexistence in 2-species communities we fix the species with biomass density B_2 at $\chi_2 = 1$ and vary the species with biomass density B_1 from $\chi_1 = 0$ to a small positive value. In other words, we reduce the gap between the two species by weakening the ability to capture light and strengthening the ability to capture water of the species that specializes in capturing light. We reduce the gap for three representative values of α : $\alpha = 1$ (diagonal curve), $\alpha < 1$ (sup-diagonal curve) and $\alpha > 1$ (sub-diagonal curve). In a species pool represented by a sup-diagonal tradeoff curve, increasing χ from zero involves a sharp increase in E , i.e. in the ability to capture water, which comes at the expense of a small decrease in K , i.e. in the ability to capture light (see point c in Fig. 1). That is, the overall competitive ability is bettered with respect to the reference case represented by the diagonal tradeoff line (point b in Fig. 1). In a species pool represented by a sub-diagonal tradeoff curve, the increase of χ involves a sharp decrease in K , which is compensated

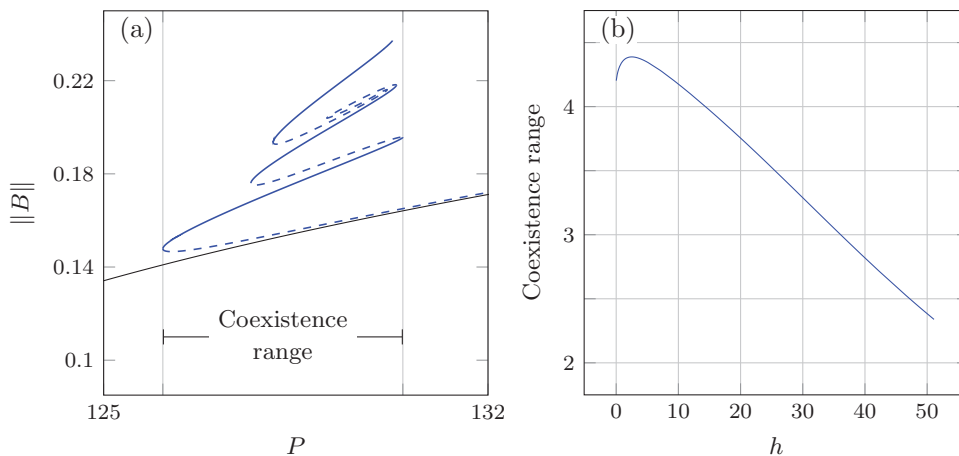


Fig. 5. Dependence of the species coexistence range, as defined by the existence range of the one-hump solution (see panel a), on the parameter h that controls the competition for light. The coexistence range decreases as h increases or as the competition for light weakens (b). Parameters are as in Table 1 with $h = 4$ in panel (a).

only by a small increase in E (point a in Fig. 1). That is, the overall competitive ability is worsened with respect to the reference case.

Fig. 6 shows the localized solution branches for three representative values of α . Two trends can be identified with respect to the reference diagonal tradeoff curve ($\alpha = 1$); the range of localized solutions moves to higher (lower) precipitation and narrows down (widens up) as α is increased (decreased). These trends can be understood by comparing the dynamics of the fronts that separate the two stable states (U_2^* and $U_{1,p}^*$) when $\alpha \neq 1$ with the front dynamics in the reference case $\alpha = 1$, as explained below. Recall that at precipitation rates below (above) the range of localized solutions the χ_2 (χ_1) species displaces by front propagation the χ_1 (χ_2) species.

When $\alpha > 1$ the species χ_1 is significantly less competitive in capturing light compared to the reference case $\alpha = 1$ because of its smaller K value. It is also less competitive in capturing water

because it is significantly less better off in water capture compared with the reference case (see Fig. 1). As a result, there exists a precipitation range (just below $P = 130$ in Fig. 6) where the species χ_1 displaces χ_2 when $\alpha = 1$ but fails to displace χ_2 and forms localized structures when $\alpha > 1$. Likewise, there exists a precipitation range (around $P = 125$) where χ_2 is unable to displace χ_1 when $\alpha = 1$ but succeeds when $\alpha > 1$. This explains the shift of the localized solutions range to higher P as α increases beyond unity. It also explains the narrowing down of the localized solutions range because the advantage of χ_2 over χ_1 is stronger at lower P than the converse advantage at higher P and therefore the contraction of the localized solutions range at the lower P edge is larger than the extension of the range at the upper P edge. Similar arguments explain the shift of the localized solutions range to lower P and its widening as α decreases below unity.

Finally, we note that if we reduce the gap between the two species by fixing $\chi_1 = 0$ and decreasing slightly χ_2 away from unity along the different trait curves, using again the diagonal ($\alpha = 1$) as a reference curve, the effect on the localized solutions range compared to Fig. 6 is qualitatively the same with respect to the widening of the localized solutions range, while it is the inverse with respect to the shift of the range.

6. Conclusion

We used a spatially explicit mathematical model to study conditions for spatial coexistence of two plant species that make different tradeoffs in capturing two limiting resources, soil water and sun light. We focused on a parameter regime that gives rise to bistability of two pure-population states over a range of precipitation rates: a uniform state of a species that specializes in capturing water and a patterned state of a species that specializes in capturing light. Within the bistability range we identified a sub-range where localized solutions exist, describing fixed domains of the patterned states in a system otherwise occupied by the uniform state. Stable solutions of this kind imply long-term spatial coexistence of the two species. We found that the size of the coexistence precipitation range size reduces as the competition for light becomes weaker. We further found that the size of this range and its position along the precipitation axis vary with the form of the tradeoff curve, which defines the nature of the species pool.

Localized structures in bistability ranges of uniform and patterned states have been found in various physical contexts (Knobloch, 2008), and are likely to occur in ecological contexts too. The context considered in this paper, i.e. a plant community distributed along a tradeoff axis of above-ground vs. below-ground resource-capture capabilities, may be applicable to herbaceous plant communities in which one or more species are capable of forming patterns (Sheffer et al., 2007; Meron et al., 2007). Woody-herbaceous systems, such as Savanna landscapes (Sankaran et al., 2004), provide another possible example. Here, the pattern-forming woody life form constitutes the stable periodic-pattern state and the herbaceous vegetation forms the alternative stable uniform state – the grassland (Gilad et al., 2007a). Localized structures consisting of confined domains of the woody pattern in an otherwise uniform grassland then create savanna-like landscapes. A related problem is shrubland-grassland transitions, e.g. the displacement of black grama (*Bouteloua eriopoda*) grassland by creosotebush (*Larrea tridentata*) shrubland (Turnbull et al., 2010). Here, the displacement process is a front propagation problem, which indicates the possible realization of pinned fronts and localized structures under different environmental conditions. In all these examples identifying bistability ranges of uniform and patterned population states may shed new light on the possible dynamical responses of the corresponding plant communities to

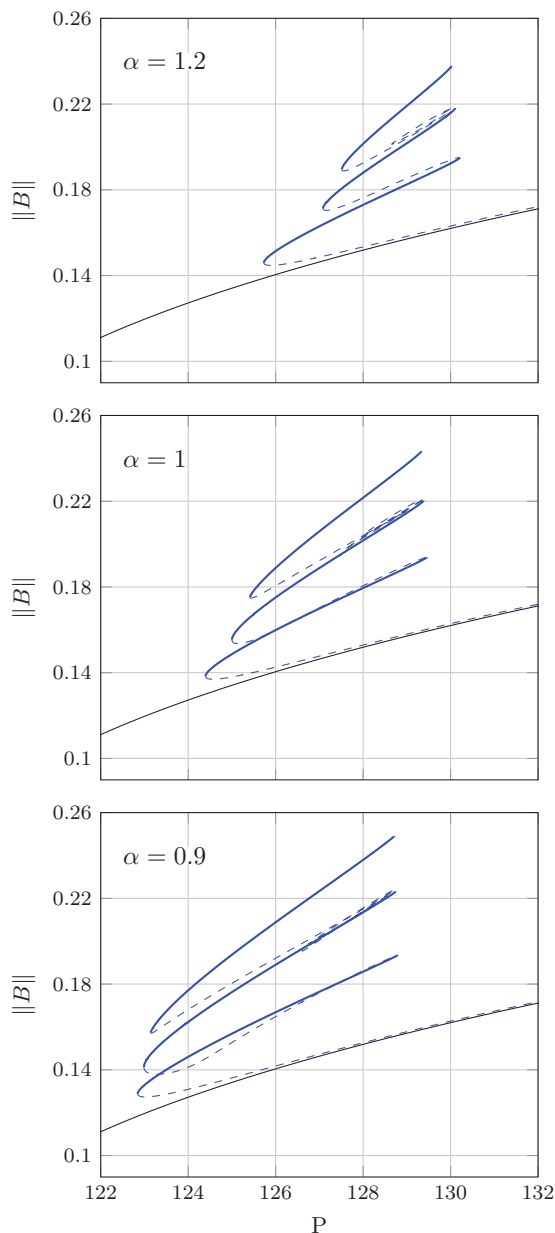


Fig. 6. Species-pool effects on the species-coexistence range. The range moves to higher (lower) precipitation and narrows down (widens up) as α is increased (decreased) with respect to the reference value $\alpha = 1$. Parameters are as in Table 1 with $\chi_1 = 0.01$.

environmental changes. We note that the assumption of sandy soil, which we used to simplify the model equations by eliminating overland water flow, applies to several examples of pattern-forming herbaceous and woody-herbaceous systems, e.g. herbaceous gap patterns (fairy circles) (Cramer and Barger, 2013) and savanna landscapes (Scholes et al., 2002) in southern Africa. We believe, however, that the coexistence mechanism is general and applies to other soil types in bistability ranges of uniform and patterned vegetation states.

A basic assumption underlying the model equations is translational invariance, that is, the absence of any external heterogeneity, such as non-uniform rainfall. Such heterogeneities can lead to front pinning and species coexistence even in the case of bistability of uniform states; a non-uniform rainfall that shifts the precipitation rate from one side of the Maxwell point to another can lead to front pinning at the spatial location of the Maxwell point. The significance of the results reported here is that front pinning and species coexistence can occur even in uniform (translationally invariant) systems. In the current study the precipitation range of species coexistence is pretty narrow. Further studies are needed in order to identify biotic and abiotic circumstances that lead to wider coexistence ranges.

Acknowledgements

We wish to thank Yuval Zelnik for his assistance in applying the numerical continuation method. Paris Kyriazopoulos would also like to thank Danielle Hilhorst for her advices during his one year stay at Université de Paris-Sud. This research has been supported by the Israel Science Foundation under Grant No. 861/09, and by the ITN FIRST of the Seventh Framework Programme of the European Community under Grant agreement No. 238702.

Appendix A. Uniform steady states and their stability properties

A.1. Uniform steady states

We focus in this appendix on the trivial uniform state, $U_0 = (0, 0, W_0)$ with $W_0 = P/L$, and on the two pure-population uniform states $U_1^* = (B_1^*, 0, W_1^*)$ and $U_2^* = (0, B_2^*, W_2^*)$ for $B_1^*, B_2^* > 0$. We do not study mixed states of the form (B_1, B_2, W) as they are unstable in the parameter range we consider in this study.

The uniform pure-population states, for $i = 1, 2$, are given by

$$B_i^{*\pm} = \frac{\pm\sqrt{\Delta_i} + P\Omega_i(K_iE_i - 1) - \Gamma_iK_iM_i}{2E_i(\Gamma_iK_iM_i + P\Omega_i)},$$

and

$$W_i^{*\pm} = \frac{P}{L + \Gamma_iB_i^{*\pm}(1 + E_iB_i^{*\pm})},$$

with

$$\Delta_i(P) = (K_i(\Gamma_iM_i - PE_i\Omega_i) + P\Omega_i)^2 - 4K_iE_i(LM_i - P\Omega_i)(\Gamma_iK_iM_i + P\Omega_i),$$

where a necessary condition for these states to exist is Δ_i being non-negative. Let,

$$P_i^0 := LM_i/\Omega_i \tag{A.1}$$

and

$$P_i^F := \frac{M_i(2K_iE_i\sqrt{L\Gamma_iK_i(K_iE_i + 1) + L^2} - K_i(\Gamma_i - 2LE_i) - \Gamma_iK_i^2E_i)}{\Omega_i(K_iE_i + 1)^2}, \tag{A.2}$$

be the largest root of $\Delta_i(P) = 0$. Note that $B_i^{*\pm}$ is a double root at P_i^F and $d^2/dP^2(\Delta_i(P)) > 0$ which implies that $\Delta_i(P) > 0$ for $P > P_i^F$. Therefore, if

$$(K_iE_i - 1) > 0 \text{ and } P_i^F\Omega_i(K_iE_i - 1) - \Gamma_iK_iM_i > 0, \tag{A.3}$$

$$B_i^{*\pm} > 0, \text{ for } P_i^F \leq P < P_i^0, \tag{A.4}$$

and

$$B_i^{*-} \leq 0 < B_i^{*+}, \text{ for } P \geq P_i^0. \tag{A.5}$$

On the other hand, when (A.3) is not satisfied, B_i^{*+} is positive for $P > P_i^0$ while B_i^{*-} is negative for all $P > P_i^F$. We use these criteria to define parameter ranges where $U_i^{*\pm} = (B_i^{*\pm}, 0, W_i^{*\pm})$ ($i = 1, 2$) are positive, and thus can represent realistic quantities. In what follows, we refer to $U_i^{*\pm}$ only in parameter ranges where they are positive.

A.2. Stability

To study the stability of a uniform state U^* to uniform and nonuniform perturbation we consider an unbounded domain and an infinitesimally small sinusoidal perturbation with wavenumber k :

$$U(x, t) = U^* + \hat{U}\exp(ikx + \lambda t) + c.c., \tag{A.6}$$

where $U(x, t) = (B_1(x, t), B_2(x, t), W(x, t))$ represents the perturbed state and ‘‘c.c.’’ stands for the complex conjugate. We then study the linear problem obtained by inserting the form (A.6) into (2.1) keeping only terms that are linear in \hat{U} .

To simplify the presentation, we first study the stability of U^* to uniform perturbations for which $k = 0$. In this case, the linear stability of U^* is determined by the eigenvalues of a 3×3 Jacobian matrix associated with the reaction terms of (2.1). For the trivial uniform state $U^* = U_0$ the Jacobian reads,

$$J^0(0, 0, W_0) = \begin{pmatrix} P\Omega_i/L - M_i & 0 & 0 \\ 0 & P\Omega_i/L - M_i & 0 \\ -\Gamma_iP/L & -\Gamma_iP/L & -L \end{pmatrix} \tag{A.7}$$

which readily implies that U_0 is stable for $P < P_0 := \min\{P_1^0, P_2^0\}$, where P_1^0, P_2^0 are given by (A.1), and becomes unstable for $P > P_0$.

For the pure uniform states, $U_1^{*\pm}$ and $U_2^{*\pm}$, the corresponding Jacobian matrices $J^{1\pm}(B_1^{*\pm}, 0, W_1^{*\pm})$ and $J^{2\pm}(0, B_2^{*\pm}, W_2^{*\pm})$ have, respectively, the following entries:

$$\begin{aligned} J_{21}^{1\pm} &= J_{23}^{1\pm} = 0 \\ J_{11}^{1\pm} &= \Omega_1B_1^{*\pm}(E_1 - 1/K_1 - 2E_1B_1^{*\pm}/K_1)W_1^{*\pm} \\ J_{13}^{1\pm} &= \Omega_1(1 - B_1^{*\pm}/K_1)(1 + E_1B_1^{*\pm})B_1^{*\pm} \\ J_{31}^{1\pm} &= -(\Gamma_1(1 + 2E_1B_1^{*\pm})W_1^{*\pm}) \\ J_{33}^{1\pm} &= -(L + \Gamma_1B_1^{*\pm}(1 + E_1B_1^{*\pm})) \\ J_{22}^{1\pm} &= \Omega_2 \frac{h}{(B_1^{*\pm} + h)} W_1^{*\pm} - M_2 \end{aligned} \tag{A.8}$$

and

$$\begin{aligned}
 J_{12}^{\pm} &= J_{13}^{\pm} = 0 \\
 J_{22}^{\pm} &= \Omega_2 B_2^{*\pm} (E_2 - 1/K_2 - 2E_2 B_2^{*\pm}/K_2) W_2^{*\pm} \\
 J_{23}^{\pm} &= \Omega_2 (1 - B_2^{*\pm}/K_2) (1 + E_2 B_2^{*\pm}) B_2^{*\pm} \\
 J_{32}^{\pm} &= -(\Gamma_2 (1 + 2E_2 B_2^{*\pm})) W_2^{*\pm} \\
 J_{33}^{\pm} &= -(L + \Gamma_2 B_2^{*\pm} (1 + E_2 B_2^{*\pm})) \\
 J_{11}^{\pm} &= \Omega_1 \frac{h}{(B_2^{*\pm} + h)} W_2^{*\pm} - M_1.
 \end{aligned}
 \tag{A.9}$$

The stability of U_1^{\pm} and U_2^{\pm} is determined by the roots of the characteristic polynomials

$$(J_{22}^{\pm} - \lambda_1) (\lambda_1^2 - (J_{11}^{\pm} + J_{33}^{\pm}) \lambda_1 - J_{13}^{\pm} J_{31}^{\pm} + J_{11}^{\pm} J_{33}^{\pm}) = 0,
 \tag{A.10}$$

$$(J_{11}^{\pm} - \lambda_2) (\lambda_2^2 - (J_{22}^{\pm} + J_{33}^{\pm}) \lambda_2 - J_{23}^{\pm} J_{32}^{\pm} + J_{22}^{\pm} J_{33}^{\pm}) = 0.
 \tag{A.11}$$

We first examine the roots of the polynomial

$$\lambda_i^2 - (J_{ii}^{\pm} + J_{33}^{\pm}) \lambda_i + J_{ii}^{\pm} J_{33}^{\pm} - J_{i3}^{\pm} J_{3i}^{\pm} = 0.
 \tag{A.12}$$

which appears in (A.10) and (A.11) for $i = 1$ and 2 , respectively. For this we note that

$$J_{ii}^+ J_{33}^+ - J_{i3}^+ J_{3i}^+ > 0,
 \tag{A.13}$$

and

$$J_{ii}^- J_{33}^- - J_{i3}^- J_{3i}^- < 0.
 \tag{A.14}$$

To see this, recall that B_i^{\pm} are roots of the polynomial

$$f_i(s) := \Omega_i P (1 - s/K_i) (1 + E_i s) - M_i (L + \Gamma_i s (1 + E_i s)),
 \tag{A.15}$$

and note that

$$f_i'(s) = -\left(\Gamma_i M_i (2sE_i + 1) - P \Omega_i \left(-\frac{2sE_i}{K_i} - \frac{1}{K_i} + E_i \right) \right).$$

Let

$$g_i(s) := -s f_i'(s),$$

then we observe that

$$J_{ii}^+ J_{33}^+ - J_{i3}^+ J_{3i}^+ = g_i(B_i^{*+}).$$

Since $g_i'(s) = 4E_i(\Gamma_i K_i M_i + P \Omega_i)/K_i > 0$, $g_i(s)$ is convex. Moreover, $g_i(s)$ has one zero at $s = 0$ and the other coincides with the point at which $f_i(s)$ achieves a maximum. Therefore, we easily conclude that $J_{ii}^+ J_{33}^+ - J_{i3}^+ J_{3i}^+ = g_i(B_i^{*+}) > 0$ and $J_{ii}^- J_{33}^- - J_{i3}^- J_{3i}^- = g_i(B_i^{*-}) < 0$, whenever B_i^* is positive. Consequently, from (A.14) the characteristic polynomial for the linearization around U_i^{*-} , possesses at least one eigenvalue with positive real part, and thus U_i^{*-} is unstable. On the other hand, from (A.13) both eigenvalues of the linearization around U_i^{*+} , which correspond to the roots of (A.12), have negative real part when

$$(J_{ii}^+ + J_{33}^+) < 0,
 \tag{A.16}$$

for $i = 1$ or 2 .

It remains to determine the signs of the other eigenvalues that arise from (A.10) and (A.11), namely $\lambda_1 = J_{22}^{\pm}$ and $\lambda_2 = J_{11}^{\pm}$. For simplicity, we assume that

$$M_1 = M_2 \quad \text{and} \quad \Omega_1 = \Omega_2,
 \tag{A.17}$$

which is compatible with the parameter values considered in Table 1. Then,

$$\lambda_i(B_i^+; P) = \frac{P \Omega_1 h}{(B_i^+ + h)(L + \Gamma_i B_i^+ (1 + E_i B_i^+))} - M_1.$$

Moreover, the algebraic system

$$\lambda_i(s; P) = 0, \quad f_i(s; P) = 0,
 \tag{A.18}$$

with f_i given in (A.15), is solvable for a pair (s, P) . We consider the solution pair (s_i, P_i^M) with

$$s_i^* := \left(E_i K_i - 1 - E_i h + \sqrt{(E_i K_i - 1 - h E_i)^2 - 4 E_i (h(1 - E_i K_i) - K_i)} \right) (2E_i)^{-1},$$

and

$$P_i^M := M_1 (s_i^* + h) (L + \Gamma_i s_i^* (1 + E_i s_i^*)) (\Omega_1 h)^{-1}.
 \tag{A.19}$$

Then, we have that $\lambda_i(B_i^+)$ is negative for $P < P_i^M$ when

$$E_i K_i \geq 1,
 \tag{A.20}$$

or

$$E_i K_i < 1 \quad \text{and} \quad h < K_i / (1 - E_i K_i),
 \tag{A.21}$$

while it is positive for $E_i K_i < 1$, $h \geq K_i / (1 - E_i K_i)$ and $P > P_0$, or for $E_i K_i \geq 1$ and $P > P_i^M$.

We conclude that when (A.16), (A.17) along with (A.20) or (A.21) are satisfied for $i = 1$ (respectively $i = 2$), U_1^{*+} (respectively U_2^{*+}) is stable, for all $P < P_1^M$ (respectively $P < P_2^M$). On the other hand, U_i^{*-} is unstable for the range of P defined in (A.4).

We are now in a position to study the stability of the trivial state, U_0 , and of the two pure-population states, U_1^{\pm} and U_2^{\pm} , to the growth of nonuniform perturbations characterized by nonzero wavenumbers, i.e. $k \neq 0$ in (A.6). The dynamics of such perturbation are determined by the eigenvalues of the matrix

$$J_k = J - k^2 D,$$

where

$$D = \text{diag}(D_{B_1}, D_{B_2}, D_W),$$

and J is given by (A.7) for U_0 and by the expressions in (A.8) and (A.9) for U_1^{\pm} and U_2^{\pm} . The eigenvalues of J_k are determined by the roots of the characteristic polynomial:

$$\det(J - k^2 D - \lambda I_3) = 0,
 \tag{A.22}$$

where I_3 is the 3×3 identity matrix. It can be easily checked that for $P < P_0 = \min\{P_1^0, P_2^0\}$ the trivial state U_0 remains stable for all k , since the diagonal elements of J^0 in (A.7) are negative.

For the pure-population state U_1^{*+} (respectively U_2^{*+}), we assume that (A.16), (A.17) along with (A.20) or (A.21) are satisfied and that $P < P_1^M$ (respectively $P < P_2^M$), so that the state is stable for $k = 0$. For the sake of clarity, in what follows we drop superscript ‘+’ in the notation of the elements (A.8), (A.9) of the Jacobian matrix. Then, the characteristic polynomial (A.22) for the two pure-population states takes the forms

$$(J_{22}^1 - k^2 D_{B_2} - \lambda_1) (\lambda_1^2 - \alpha_1(k^2) \lambda_1 + \beta_1(k^2)) = 0, \tag{A.23}$$

$$(J_{11}^2 - k^2 D_{B_1} - \lambda_2) (\lambda_2^2 - \alpha_2(k^2) \lambda_2 + \beta_2(k^2)) = 0, \tag{A.24}$$

where

$$\alpha_i(k^2) = (J_{ii}^i + J_{33}^i) - (D_{B_i} + D_W)k^2, \tag{A.25}$$

$$\beta_i(k^2) = D_{B_i} D_W k^4 - (D_{B_i} J_{33}^i + D_W J_{ii}^i)k^2 + (J_{ii}^i J_{33}^i - J_{i3}^i J_{3i}^i). \tag{A.26}$$

Clearly the single eigenvalues $\lambda_1(k^2) = J_{22}^1 - k^2 D_{B_2}$ and $\lambda_2(k^2) = J_{11}^2 - k^2 D_{B_1}$ are negative for all k , and the other two eigenvalues are given by

$$\lambda_{i\pm}(k^2) = \frac{\alpha_i(k^2) \pm \sqrt{\alpha_i(k^2)^2 - 4\beta_i(k^2)}}{2}. \tag{A.27}$$

Since $\alpha_i(k^2) < 0$, the real part of $\lambda_{i-}(k^2)$ remains negative for all k , while λ_{i+} may become positive, only if

$$\beta_i(k^2) < 0, \tag{A.28}$$

for some $k \neq 0$. From (A.13), this immediately implies, that $(D_{B_i} J_{33}^i + D_W J_{ii}^i)$ needs to be positive, or

$$T(\delta) = \delta J_{33}^i + J_{ii}^i > 0, \quad \delta := D_{B_i} / D_W. \tag{A.29}$$

Therefore, since $J_{33}^i < 0$, destabilization of S_i^{*+} , requires

$$J_{ii}^i = \Omega_i B_i^{*+} \left(E_i - 1/K_i - 2 \frac{E_i}{K_i} B_i^{*+} \right) W_i^{*+} > 0. \tag{A.30}$$

In addition, from (A.16) $(J_{ii}^i + J_{33}^i) < 0$ and since $T(\delta) = (\delta J_{33}^i + J_{ii}^i)$ is a decreasing function of δ , we also need

$$\delta < 1. \tag{A.31}$$

Moreover, (A.26) has a minimum at

$$k_{i,c}^2 = \frac{(D_{B_i} J_{33}^i + D_W J_{ii}^i)}{2 D_{B_i} D_W}, \tag{A.32}$$

and so (A.28) is satisfied for some $k \neq 0$, when the parameter values $K_i, E_i, M_i, L, N_i, \Gamma, P$ and the diffusion coefficients D_{B_i}, D_W are such that the minimum value given by the expression

$$\beta_i(k_{i,c}^2) = 4 D_{B_i} D_W (J_{ii}^i J_{33}^i - J_{i3}^i J_{3i}^i) - (D_{B_i} J_{33}^i + D_W J_{ii}^i)^2, \tag{A.33}$$

is negative. Finally, zeros of the right hand side of (A.33) with respect to P provide us the instability thresholds denoted by P_i^T , while the wavenumber $k_{i,c}$ growing at the instability point is given by (A.32).

Appendix B. Numerical stability analysis for nonuniform stationary solutions in a finite system

We consider a reaction-diffusion system of the form:

$$\partial_t U = D \mathcal{L} U + F(U),$$

where the spatial variable x lies in the interval $[0, 1]$, $U = (U_1, U_2, U_3)$, $D = \text{diag}(D_1, D_2, D_3)$ for D_1, D_2, D_3 real positive numbers, $\mathcal{L} = \text{diag}(\partial_{xx}, \partial_{xx}, \partial_{xx})$ and

$$F(U) = (f_1(U), f_2(U), f_3(U))$$

is a differentiable vector field. We consider the system either with periodic boundary conditions or homogeneous Neumann boundary conditions.

We divide the spatial interval into the uniform grid $x_j = j \Delta x$, for $j = 0, \dots, N$, with $\Delta x = 1/N$, and we let

$$U_h = (u_1^0, \dots, u_1^N, u_2^0, \dots, u_2^N, u_3^0, \dots, u_3^N),$$

represent the vector of U evaluated at the grid nodes. Then we use the standard second order central difference approximation of the second derivative given by a 3 points stencil. This approximation can be represented by a $(N + 1) \times (N + 1)$ matrix \mathcal{A} . Consequently, we denote by $\delta \mathcal{A} = \text{diag}(D_1 \mathcal{A}, D_2 \mathcal{A}, D_3 \mathcal{A})$ the $3(N + 1) \times 3(N + 1)$ matrix approximating $D \mathcal{L}$, and by

$$F_h(U_h) = (f_1(u_1^0), \dots, f_1(u_1^N), f_2(u_2^0), \dots, f_2(u_2^N), f_3(u_3^0), \dots, f_3(u_3^N)).$$

the vector field evaluated at the node points.

We then compute the discrete Jacobian matrix of F_h , denoted by JF_h around an inhomogeneous discretized steady state $\bar{U}(x)$ ending up with a linear operator

$$\delta \mathcal{A} + JF_h|_{\bar{U}_h}.$$

Finally, we compute the spectrum of $\delta \mathcal{A} + JF_h|_{\bar{U}_h}$ using MATLAB, in order to determine the linear stability of $\bar{U}(x)$ for the system $U_h' = \delta \mathcal{A} U_h + F_h(U_h)$, with $U_h(t), F_h$ in $R^{3(N+1)}$.

References

Baudena, M., Rietkerk, M., 2013. Complexity and coexistence in a simple spatial model for arid savanna ecosystems. *Theor. Ecol.* 6 (2), 131–141, <http://dx.doi.org/10.1007/s12080-012-0165-1>.

Beck, M., Knobloch, J., Lloyd, D., Sandstede, B., Wagenknecht, T., 2009. Snakes, ladders, and isolas of localized patterns. *SIAM J. Math. Anal.* 41 (3), 936–972, <http://dx.doi.org/10.1137/080713306>.

Borgogno, F., D’Odorico, P., Laio, F., Ridolfi, L., 2009. Mathematical models of vegetation pattern formation in ecohydrology. *Rev. Geophys.* 47, RG1005.

Bortolozzo, U., Clerc, M.G., Residori, S., 2008. Local theory of the slanted homoclinic snaking bifurcation diagram. *Phys. Rev. E* 78 (September), 036214, <http://dx.doi.org/10.1103/PhysRevE.78.036214>.

Cramer, M.D., Barger, N.N., 2013. Are namibian fairy circles the consequence of self-organizing spatial vegetation patterning? *PLoS ONE* 8, e70876.

Dawes, J.H.P., 2008. Localized pattern formation with a large-scale mode: slanted snaking. *SIAM J. Appl. Dyn. Syst.* 7, 186–206.

Deblauwe, V., Barbier, N., Couteron, P., Lejeune, O., Bogaert, J., 2008. The global biogeography of semi-arid periodic vegetation patterns. *Global Ecol. Biogeogr.* 17 (November (6)), 715–723, <http://dx.doi.org/10.1111/j.1466-8238.2008.00413.x>.

Doedel, E., Paffenroth, R.C., Champneys, A.R., Fairgrieve, T.F., Kuznetsov, A., Oldeman, Y., Sandstede, B.E., Wang, B., 2002. *Auto2000*. Tech. rep. Concordia University.

Eldridge, D.J., Zaady, E.M.S., 2012. Infiltration through three contrasting biological soil crusts in patterned landscapes in the Negev, Israel. *J. Stat. Phys.* 148, 723–739.

Field, C.B., Barros, V., Stocker, T.F., Qin, D., Dokken, D.J., Ebi, L.L., Mastrandrea, M.D., Mach, K.J., Plattner, G.-K., Allen, S.K., Tignor, M., Midgley, P.M., 2013. *Managing the risks of extreme events and disasters to advance climate change adaptation: A special report of the intergovernmental panel on climate change*. Tech. rep. Cambridge University Press, Cambridge, UK and New York, NY, USA.

Gilad, E., Shachak, M., Meron, E., 2007a. Dynamics and spatial organization of plant communities in water-limited systems. *Theor. Popul. Biol.* 72, 214–230.

Gilad, E., von Hardenberg, J., Provenzale, A., Shachak, M., Meron, E., 2004. Ecosystem engineers: from pattern formation to habitat creation. *Phys. Rev. Lett.* 93 (9), 098105.

Gilad, E., von Hardenberg, J., Provenzale, A., Shachak, M., Meron, E., 2007b. A mathematical model of plants as ecosystem engineers. *J. Theor. Biol.* 244, 680–691.

Holzappel, C., Tielbörger, K., Parag, H., Kigel, J., Sternberg, M., 2006. Annual plant–shrub interactions along an aridity gradient. *Basic Appl. Ecol.* 7, 268–279.

Jones, C., Lawton, J., Shachak, M., 1994. Organisms as ecosystem engineers. *Oikos* 69, 373–386.

- Jones, C., Lawton, J., Shachak, M., 1997. Positive and negative effects of organisms as ecosystem engineers. *Ecology* 78, 1946–1957.
- Knobloch, E., 2008. Spatially localized structures in dissipative systems: open problems. *Nonlinearity* 21 (4), T45.
- Lejeune, O., Tlidi, M., Couteron, P., 2002. Localized vegetation patches: a self-organized response to resource scarcity. *Phys. Rev. E* 66 (1), 10901.
- Maestre, F., Valladares, F., Reynolds, J., 2005. Is the change of plant–plant interactions with abiotic stress predictable? A meta-analysis of field results in arid environments. *J. Ecol.* 93, 748–757.
- Meron, E., 2011. Modeling dryland landscapes. *Math. Model. Nat. Phenom.* 6, 163–187.
- Meron, E., 2012. Pattern-formation approach to modelling spatially extended ecosystems. *Ecol. Model.* 234, 70–82.
- Meron, E., Yizhaq, H., Gilad, E., 2007. Localized structures in dryland vegetation: forms and functions. *Chaos* 17 (037109).
- Nathan, J., von Hardenberg, J., Meron, E., 2013. Spatial instabilities untie the exclusion-principle constraint on species coexistence. *J. Theor. Biol.* 335, 198–204.
- Pismen, L., 2006. *Patterns and Interfaces in Dissipative Dynamics*. Springer Series in Synergetics. Springer.
- Pomeau, Y., 1986. Front motion, metastability and subcritical bifurcations in hydrodynamics. *Physica D* 23, 3–11.
- Pugnaire, F.I., Luque, M.T., 2001. Changes in plant interactions along a gradient of environmental stress. *Oikos* 93, 42–49.
- Rietkerk, M., Boerlijst, M.C., van Langevelde, F., HilleRisLambers, R., van de Koppel, J., Kumar, L., Prins, H.H.T., Roos, A.M.D., 2002. Self-organization of vegetation in arid ecosystems. *Am. Nat.* 160, 524–530.
- Rietkerk, M., van de Koppel, J., 2008. Regular pattern formation in real ecosystems. *Trends Ecol. Evol.* 23 (3), 169–175.
- Sankaran, M., Ratnam, J., Hanan, N.P., 2004. Tree-grass coexistence in savannas revisited – insights from an examination of assumptions and mechanisms invoked in existing models. *Ecol. Lett.* 7 (6), 480–490. <http://dx.doi.org/10.1111/j.1461-0248.2004.00596.x>.
- Scholes, R., Dowty, P., Caylor, K., Parsons, D., Frost, P., Shugart, H., 2002. Trends in savanna structure and composition along an aridity gradient in the Kalahari. *J. Veg. Sci.* 13, 419–428.
- Shachak, M., Gosz, J.R., Perevolotsky, A., Pickett, S.T.A., 2005. *Biodiversity in Drylands: Towards a Unified Framework*. Oxford University Press.
- Sheffer, E., von Hardenberg, J., Yizhaq, H., Shachak, M., Meron, E., 2013. Emerged or imposed: a theory on the role of physical templates and self-organisation for vegetation patchiness. *Ecol. Lett.* 16 (2), 127–139. <http://dx.doi.org/10.1111/ele.12027>.
- Sheffer, E., Yizhaq, H., Gilad, E., Shachak, M., Meron, E., 2007. Why do plants in resource deprived environments form rings? *Ecol. Complex.* 4, 192–200.
- Tilman, D., 1982. Resource competition and community structure. In: *Monographs in Population Biology*. Princeton University Press, Princeton, NJ, USA.
- Tongway, D.J., Valentin, C., Seghier, J., Menaut, J.-C. (Eds.), 2001. *Banded Vegetation Patterning in Arid and Semiarid Environments: Ecological Processes and Consequences for Management*. Ecological Studies 149. Springer.
- Turing, A., 1952. The chemical basis of morphogenesis. *Philos. Trans. R. Soc. Lond. Ser. B* 237, 37–72.
- Turnbull, L., Wainwright, J., Brazier, R.E., 2010. Changes in hydrology and erosion over a transition from grassland to shrubland. *Hydrol. Process.* 24 (4), 393–414. <http://dx.doi.org/10.1002/hyp.7491>.
- von Hardenberg, J., Kletter, A.Y., Yizhaq, H., Nathan, J., Meron, E., 2010. Periodic versus scale-free patterns in dryland vegetation. *Proc. Roy. Soc. B* 277, 1771–1776.
- von Hardenberg, J., Meron, E., Shachak, M., Zarmi, Y., 2001. Diversity of vegetation patterns and desertification. *Phys. Rev. Lett.* 87, 198101–198111.
- Zelnik, Y.R., Kinast, S., Yizhaq, H., Bel, G., Meron, E., 2013. Regime shifts in models of dryland vegetation. *Philos. Trans. R. Soc. A* 371, 20120358.